



Published in final edited form as:

Proc SPIE Int Soc Opt Eng. 2016 February 27; 9784: . doi:10.1117/12.2216255.

Combining Population and Patient-Specific Characteristics for Prostate Segmentation on 3D CT Images

Ling Ma^{a,b}, Rongrong Guo^a, Zhiqiang Tian^a, Rajesh Venkataraman^c, Saradwata Sarkar^c, Xiabi Liu^b, Funmilayo Tade^a, David M. Schuster^a, and Baowei Fei^{*,a,d,e}

^aDepartment of Radiology and Imaging Sciences, Emory University, Atlanta, GA

^bSchool of Computer Science, Beijing Institute of Technology, Beijing

^cDepartment of R&D, Eigen, Grass Valley, CA

^dWinship Cancer Institute of Emory University, Atlanta, GA

^eThe Wallace H. Coulter Department of Biomedical Engineering, Georgia Institute of Technology and Emory University, Atlanta, GA

Abstract

Prostate segmentation on CT images is a challenging task. In this paper, we explore the population and patient-specific characteristics for the segmentation of the prostate on CT images. Because population learning does not consider the inter-patient variations and because patient-specific learning may not perform well for different patients, we are combining the population and patient-specific information to improve segmentation performance. Specifically, we train a population model based on the population data and train a patient-specific model based on the manual segmentation on three slice of the new patient. We compute the similarity between the two models to explore the influence of applicable population knowledge on the specific patient. By combining the patient-specific knowledge with the influence, we can capture the population and patient-specific characteristics to calculate the probability of a pixel belonging to the prostate. Finally, we smooth the prostate surface according to the prostate-density value of the pixels in the distance transform image. We conducted the leave-one-out validation experiments on a set of CT volumes from 15 patients. Manual segmentation results from a radiologist serve as the gold standard for the evaluation. Experimental results show that our method achieved an average DSC of 85.1% as compared to the manual segmentation gold standard. This method outperformed the population learning method and the patient-specific learning approach alone. The CT segmentation method can have various applications in prostate cancer diagnosis and therapy.

Keywords

prostate; image segmentation; CT; population characteristics; patient-specific characteristics

* bfei@emory.edu ; Website: <http://feilab.org>.

1. INTRODUCTION

Prostate cancer is the second leading cause of cancer mortality in American men.¹ In radiotherapy planning for prostate cancer, segmenting the prostate is a critical step. Segmentation methods of the prostate on MRI and TURS images have been developed.²⁻⁵ Prostate segmentation on CT images is a challenging task because of its lower image contrast and because of the variability of appearance of prostates for different patients. Manual segmentation from CT images is time-consuming and relies upon the experience of the clinician. There are clinical needs to develop automatic or semi-automatic segmentation methods for the prostate on CT images. Since a priori knowledge can help interpret new data, segmentation algorithms supported by supervised learning can work better than simple unsupervised solutions.

By analyzing the population of manually delineated CT images, some approaches built shape models of the prostate,^{6,7} learned the appearance characteristics,^{6,8} and learned distance transform,⁹ to guide the prostate segmentation. Since shape variation in the same patient is generally much less as compared to that of different patients, some works learned the patient-specific appearance characteristics from a series of CT images from the same patient under treatment planning image.¹⁰⁻¹⁴ However, not all knowledge learned from the population is useful for segmenting the prostate of a new patient due to the specificity of each patient. Learning using only patient-specific data often suffers from overfitting. In order to address this problem, several combination approaches have been proposed. Feng et al.¹⁵ used profile-based gradient features and the local-region based probability distribution function from the population and patient-specific information to build an appearance model. They then used the active shape model with the appearance model to segment the prostate. Liao et al.¹⁶ extracted and selected salient features to localize the prostate. Then they used an online learning mechanism to adaptively integrate both the inter-patient and patient-specific information to optimize the localization accuracy. Liao et al.¹⁷ learned informative anatomical features at selected regions in the training images obtained from the population and the current treatment images. The feature selection step can help filter the regions filled with bowel gas and localize the prostate. Part et al.¹⁸ utilized a priori knowledge of population data and the patient-specific information from user interactions to estimate confident prostate voxels, background voxels, and unconfident voxels. Based on the confident voxels, they selected discriminative features for semi-supervised learning in order to predict the labels of unconfident voxels. Gao et al.¹⁹ proposed a novel learning framework. They trained a population-based discriminative appearance model, and “personalize” the model to fit the patient-specific appearance characteristics by backward pruning to discard obsolete population-based knowledge and by forward learning to incorporate patient-specific characteristics.

We propose a novel prostate segmentation method by capturing the population and patient-specific (PPS) characteristics. In this method, the user selects the base, apex and mid-gland slices and draws the contour of the prostate on the three slices as the patient-specific information. We illustrate our novel methodology in Fig. 1, where P_model and PS_model means the knowledge learned from the population and patient-specific information, respectively, and NP represents the new patient to be segmented. Instead of either preserving

or discarding the knowledge learned from the population, we use the applicable population knowledge on the specific patient to guide the prostate segmentation.

2. METHOD

For a given patient, the user selects three slices, which are base, apex and mid-gland slices, and then draws the contours of the prostate on the three slices for the patient-specific information. Combined with the population information, we can capture the characteristics which are adapted for the prostate segmentation in the specific patient. Fig. 2 shows the flowchart of the proposed method that includes two stages: i) Training stage and ii) Segmentation stage. In the training stage, we extract the discriminate features to construct the population and patient-specific models. In the segmentation stage, we explore the relationship between the population and patient-specific information to capture the population and patient-specific characteristics for prostate-likelihood prediction. Finally, we extract the prostate density in the distance transform image to achieve a smooth segmented prostate.

2.1 Feature Extraction

For each pixel in the population data and specific patient data, we extract six different types of features. These features include 1) The pixel intensity. Intensity feature can indicate the local spatial variation in the boundary. 2) The histogram of CT values over a 3×3 window centered at the pixel. It can reflect the statistic probabilistic distribution of density values in a block and is invariant in scale, rotation and translation. 3) Multi-scale rotation invariant local binary pattern (LBP). The LBP feature is a compact texture descriptor in which each comparison result between the center pixel and one of its surrounding neighbors is encoded as a bit. The neighborhood (P, R), where P represents the number of sampling points and R is the radius of the neighborhood, can be defined flexibly. In our paper, we set the ranges of P and R for calculating LBP feature to be {4, 5} and {1, 2}, respectively, for a multi-scale LBP features. In each scale, we choose the minimum value as the LBP value by rotating each bit pattern circularly for the rotation invariant. 4) Gray-level co-occurrence matrix (GLCM). The GLCM feature is a statistical tool for extracting second-order texture information from images. 5) Histogram of oriented gradient (HOG). The HOG feature is a texture descriptor describing the distribution of image gradients in different orientations. We extract the HOG feature from a 16×16 window centered at each pixel. We divide the window into smaller rectangular blocks of 8×8 pixels and further divide each block into 4 cells of 4×4 pixels. For each cell, we compute the orientation histogram which contains 9 bins covering a gradient orientation range of 0° – 180° . The histogram can then be represented by the linking of all the orientation histograms. 6) Haar-like features. The Haar-like feature is a regional characteristic based on gray distribution.

2.2 Classifier Training

The Adaboost classifier²⁰ is an ensemble classifier which combines many other types of classifiers to improve their performance. Since it can converge to a strong learner by combining a sequence of weak classifiers by dynamically adjusting the weights of each

classifier according to the errors in the previous learning step, it is commonly used in medical image classification.

We employ the Adaboost method with a decision tree method as the weak classifier to train the population data and patient-specific data. For the population learning, we extract the features described in Section 2.1 for each pixel in the training images and use the labels to train the Adaboost classifier. For the patient-specific learning, we use the user interaction to obtain the patient-specific information. The user selects the base, apex and mid-gland slices and segments the prostate contours on these slices. Based on the label of each pixel on the three slices, we extract its features and train three Adaboost classifiers for modeling the patient-specific prostate. During the training stage, we obtain four classifiers: Adaboost for population knowledge and Adaboost for patient-specific knowledge on the base (Ada_B), mid-gland (Ada_M) and apex (Ada_A) slices.

2.3 Prostate-Likelihood Prediction by Combining the Population and Patient-Specific Characteristics

Since inter-patient variations can be large, the learned population characteristics are not completely applicable to the patient-specific data. We can obtain patient-specific knowledge by using the data on the three slices. We then combine the patient-specific characteristics with the general population statistics. Specifically, we compute the similarity between the population and patient-specific models to combine the population and patient-specific characteristics for more accurate segmentation. Because the label of every pixel on the base, mid-gland and apex slices has been marked by the user, the goal of this segmentation method is to predict the label of every pixel on the other slices. Let $P_B(i)$, $P_M(i)$ and $P_A(i)$ be the probability of the pixel i predicted by the model Ada_B, Ada_M and Ada_A, $S(T,B)$, $S(T,M)$ and $S(T,A)$ be the similarity between the population model and the patient-specific model on the base, mid-gland and apex slices, respectively. The final probability of belonging to the prostate for the pixel i , $P(i)$, is computed by

$$P(i) = S(T, B) P_B(i) + S(T, M) P_M(i) + S(T, A) P_A(i). \quad (1)$$

For the given model X and Y, the $S(X, Y)$ is determined by

$$S(X, Y) = \sum_{k \in D_Y} \frac{AND(L_X(k), True(k))}{N_Y}, \quad (2)$$

where D_Y means the data set, *i.e.*, the pixel set that are used to train the model Y, N_Y means the number of pixels belonging to the prostate, $L_X(k)$ and $True(k)$ are the label predicted by the model X and the true label of the pixel k, respectively; and $AND(L, T)$ is a function measuring the similarity between the two labels, which is described below.

$$AND(L, T) = \left\{ \begin{array}{l} 1, \text{ if } T \text{ belongs to the prostate and } L \text{ is classified as the prostate} \\ 0 \text{ others} \end{array} \right\}.$$

(3)

In Eq.1, we multiply the probability obtained from the patient-specific model by the similarity of the population and patient-specific model, and use the product as the probability of the pixel belonging to the prostate. The similarity between the two models reflects the proportion of the general population knowledge which is applicable to the specific patient. The product can address the influences of applicable population on the specific patient and then fuse the population and patient-specific characteristics for more accurately computing the probability. We then combine the probability obtained from the three patient-specific models into a sum to represent the final probability in order to improve the stability and accuracy. We use zero as the threshold to achieve a segmented prostate mask.

2.4 Surface Smoothness by Prostate-Density based on Distance Transform

We use the prostate-density based on distance transform to filter the scattered points and smooth the surface of the prostate. Prostate-density is the density of prostate pixels in a block, while the distance transform can convert a binary image into another image where each object pixel has a value corresponding to the minimum distance from the background. We find the maximum value of the pixel in the distance transform image, represented by *VALUE_MAX*, and divide each pixel value by the *VALUE_MAX* to normalize the distance transform image. We then use the sum of the value of the pixels in its neighboring (5×5) block, as the prostate density of the pixel *i*, as described below

$$PD(i) = \sum_{j \in block} DT(j), \quad (4)$$

where $DT(j)$ means the value of the pixel *j* in the normalized distance transform image and *j* is the neighbor of *i*. The prostate density of the pixel is very low if it is a scattered point. Hence, we can filter the scattered points whose prostate density is smaller than a fixed threshold. We can further smooth the segmented prostate by adjusting the threshold.

2.5 Evaluation Criterion

To evaluate the performance of the segmentation, ²¹ Dice similarity coefficient (DSC), sensitivity, specificity and overlap error (OVE) were investigated in the segmentation experiment. Let *S* and *G* be the binary masks from our method and the manual segmentation by a radiologist, respectively. DSC is the relative volume overlap between *S* and *G*. It is can be computed by

$$DSC = \frac{2 \times TP}{(FP+TP) + (TP+FN)}, \quad (5)$$

where TP, TN, FP, FN is the number of true positives, true negatives, false positives and false negatives, respectively. If a prostate pixel can be classified as a prostate pixel correctly, we call it “true positive”. If a prostate pixel can be classified as a non-prostate incorrectly, we call it “false negative”. In the same way, “true negative” means that a non-prostate pixel can be recognized into non-prostate correctly whereas “false positive” means that a non-prostate pixel is recognized into prostate incorrectly.

Sensitivity (SE) measures the proportion of prostate pixels which are correctly identified as the prostate while specificity (SP) measures the proportion of non-prostate pixels which are correctly identified as non-prostate. They are determined by:

$$\begin{aligned} \text{Sensitivity} &= \frac{TP}{TP+FN} \\ \text{Specificity} &= \frac{TN}{TN+FP} \end{aligned} \quad (6)$$

Overlap error (OVE) is an evaluation criterion of errors, as described below.

$$OVE = 1 - \frac{S \cap G}{S \cup G} \quad (7)$$

3. EXPERIMENT

3.1 Databases

CT image volumes from 15 patients were used in the segmentation experiments. All the prostate CT images were from a PET/CT scanner and the volumetric data are saved slice by slice in the DICOM format. The slice thickness is 4.25 mm and the size of the images is $512 \times 512 \times 103$ voxels. The in-plane resolution is $0.977 \times 0.977 \text{ mm}^2$. The prostate was manually segmented by an experienced radiologist to produce the gold standard for evaluation. We conducted leave-one-out style cross-validation experiments for the prostate segmentation.

3.2 Visualization Assessment

For four slices that were randomly chosen from the prostate volume except the base, apex and mid-gland slices, the segmented results are as shown in Fig. 3, indicating good match between the computer and manual segmentations.

3.3 Segmentation Performance

The segmented results for 15 patient data are shown in Table 1. Our approach achieved an average DSC of $85.1 \pm 0.26\%$ with the minimal DSC of 75.3% and the maximum DSC of 91.1%, an average sensitivity of $83.3 \pm 1.10\%$ with the minimal sensitivity of 64.5% and the

maximum sensitivity of 98.3%, an average specificity of $91.5 \pm 0.52\%$, with the minimal one, 73.2%, and the maximum one, 98.9%, and an average overlap error of $25.6 \pm 0.56\%$, with the lowest one, 16.3%, and the highest one, 39.6%. These results show that our method can achieve a good segmentation performance.

3.4 Comparison between our Method and Population Learning and Patient-Specific Learning Methods

To illustrate the effectiveness of our method, we compare it with the two learning methods: the population learning (P_L) alone and the patient-specific learning (PS_L) alone. P_L trains the Adaboost classifier only on the population data while PS_L trains the classifier only on the patient-specific data. According to the trained classifier, P_L and PS_L methods recognize the class (prostate or non-prostate) of each pixel to complete the prostate segmentation. In our experiments, we conduct the leave-one-out style cross-validation experiments to segment the prostate for the 15 patient data by using the P_L method, PS_L method, and our PPS method. The results are shown in Fig. 4. The DSC and sensitivity from our method are highest among the three methods and the overlap error is the lowest. Although our specificity is not the highest one but still achieve an average sensitivity of 91.5%. These results demonstrate that our method can take the advantages of combining the population and patient-specific characteristics but overcome their related weaknesses.

4. CONCLUSIONS

In this paper, a semi-automatic segmentation method has been proposed to segment the prostate on CT images. The method not only learns a discriminative model based on the population data but also uses the user interaction information to learn a patient-specific model. The two models are combined together to capture the applicable population characteristics on the specific patient for improving the segmentation performance. A new surface smoothness method based on the prostate-density in the distance transform image is involved to improve the segmentation performance. The experimental results show that our method achieved a satisfactory performance. Moreover, compared with population learning or patient-specific learning method alone, the proposed method performs better in capturing patient-specific appearance characteristics from limited patient-specific data and large population data for more accurate segmentation. Our prostate CT segmentation method can be suitable for various applications in prostate cancer diagnosis and therapy.

5. ACKNOWLEDGEMENTS

This research is supported in part by NIH grants (CA176684 and CA156775). LM was partially supported by International Graduate Exchange Program of Beijing Institute of Technology. XL was partially supported by National Natural Science Foundation of China (Grant no. 60973059, 81171407) and the Program for New Century Excellent Talents in Universities of China (Grant No. NCET-10-0044). The work was conducted in the Quantitative BioImaging Laboratory in the Emory Center for Systems Imaging (CSI) of Emory University School of Medicine.

REFERENCES

- [1]. Siegel RL, Miller KD, Jemal A. Cancer statistics, 2015. *CA: a cancer journal for clinicians*. 2015; 65(1):5–29. [PubMed: 25559415]

- [2]. Tian Z, et al. Superpixel-based Segmentation for 3D Prostate MR Images. *IEEE Trans Med Imaging*. Oct 30.2015 Epub ahead of print] PubMed, PMID: 26540678.
- [3]. Akbari H, Fei B. 3D ultrasound image segmentation using wavelet support vector machines. *Med Phys*. 2012; 39(6):2972–84. [PubMed: 22755682]
- [4]. Fei B, et al. A Molecular Image-directed, 3D Ultrasound-guided Biopsy System for the Prostate. *Proc SPIE Int Soc Opt Eng*. 2012:831613–831613. [PubMed: 22708023]
- [5]. Yang X, Fei B. 3D Prostate Segmentation of Ultrasound Images Combining Longitudinal Image Registration and Machine Learning. *Proc SPIE Int Soc Opt Eng*. 2012; 8316:83162O–83162O.
- [6]. Tang X, et al. Geometric-model-based segmentation of the prostate and surrounding structures for image-guided radiotherapy. *International Society for Optics and Photonics in Electronic Imaging*. 2004:168–176.
- [7]. Martínez F, et al. Segmentation of pelvic structures for planning CT using a geometrical shape model tuned by a multi-scale edge detector. *Physics in medicine and biology*. 2014; 59(6):1471. [PubMed: 24594798]
- [8]. Nguyen HG, et al. Automatic 3D seed location and orientation detection in CT image for prostate brachytherapy. *IEEE 11th International Symposium on Biomedical Imaging ISBI*. 2014:1320–1323.
- [9]. Gao Y, et al. Learning distance transform for boundary detection and deformable segmentation in ct prostate images. *Machine Learning in Medical Imaging*. 2014:93–100.
- [10]. Li W, et al. Learning image context for segmentation of the prostate in CT-guided radiotherapy. *Physics in Medicine and Biology*. 2012; 57(5):1283–1308. [PubMed: 22343071]
- [11]. Wu Y, et al. Prostate Segmentation based on Variant Scale Patch and Local Independent Projection. *IEEE Transactions on Medical Imaging*. 2014; 33(6):1290–1303. [PubMed: 24893258]
- [12]. Shi Y, et al. Prostate Segmentation in CT Images via Spatial-Constrained Transductive Lasso. *Proceedings of the IEEE Conference on Computer Vision and Pattern Recognition CVPR*. 2013:2227–2234.
- [13]. Liao S, Gao Y, Shen D. Sparse patch based prostate segmentation in CT images. *Medical Image Computing and Computer-Assisted Intervention–MICCAI*. 2012:385–392.
- [14]. Shi Y, et al. Transductive prostate segmentation for CT image guided radiotherapy. *Machine Learning in Medical Imaging*. 2012:1–9.
- [15]. Feng Q, et al. Segmenting CT prostate images using population and patient-specific statistics for radiotherapy. *Medical Physics*. 2010; 37(8):4121–4132. [PubMed: 20879572]
- [16]. Liao S, Shen D. A learning based hierarchical framework for automatic prostate localization in CT images. *Image Analysis and Image-Guided Interventions in Prostate Cancer Imaging*. 2011:1–9.
- [17]. Liao S, Shen D. A feature-based learning framework for accurate prostate localization in CT images. *IEEE Trans Image Process*. 2012; 21(8):3546–59. [PubMed: 22510948]
- [18]. Park SH, et al. Interactive prostate segmentation using atlas-guided semi-supervised learning and adaptive feature selection. *Medical physics*. 2014; 41(11):111715. [PubMed: 25370629]
- [19]. Gao Y, Zhan Y, Shen D. Incremental learning with selective memory (ILSM): Towards fast prostate localization for image guided radiotherapy. *IEEE Transactions on Medical Imaging*. 2014; 33(2):518–534. [PubMed: 24495983]
- [20]. Freund Y, Schapire RE. Experiments with a new boosting algorithm. *ICML*. 1996; 96:148–156.
- [21]. Ghose S, et al. A survey of prostate segmentation methodologies in ultrasound, magnetic resonance and computed tomography images. *Computer methods and programs in biomedicine*. 2012; 108(1):262–287. [PubMed: 22739209]

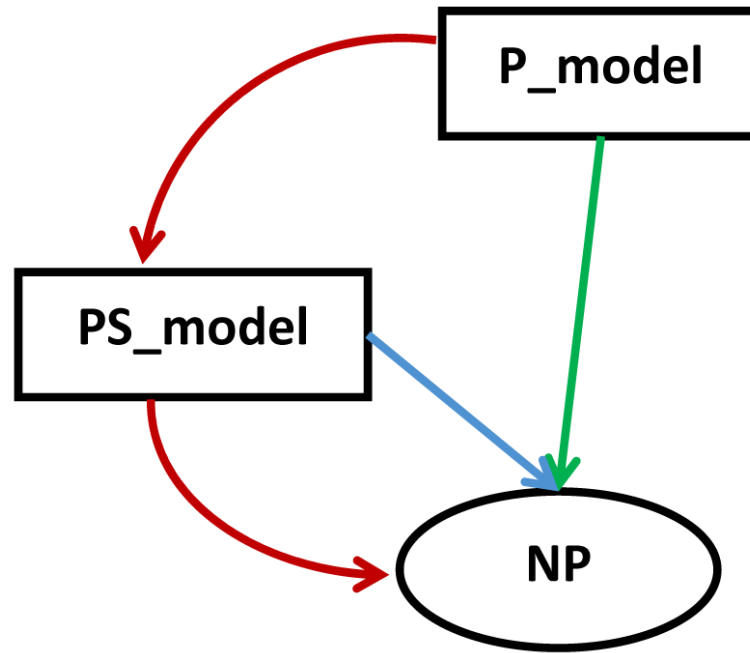


Fig. 1. The illustration of pure population learning method (green line), patient-specific learning (blue line), and our method (red line).

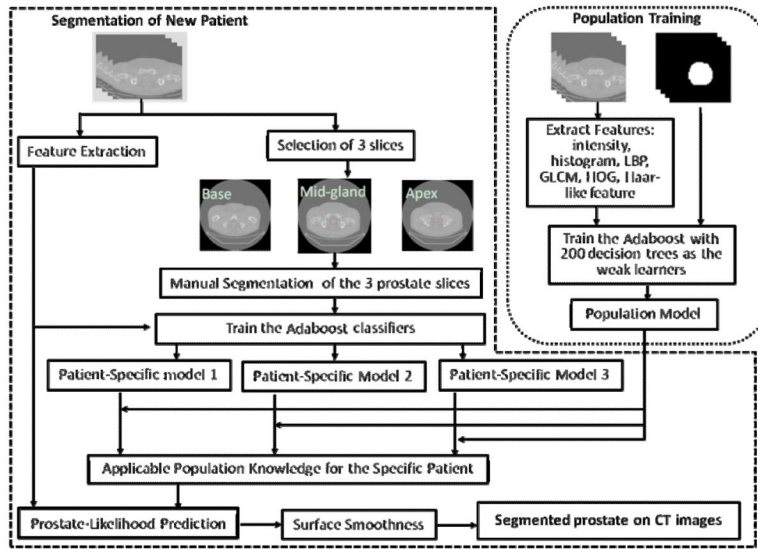


Fig. 2. Flowchart of the segmentation method based on the population and patient-specific characteristics

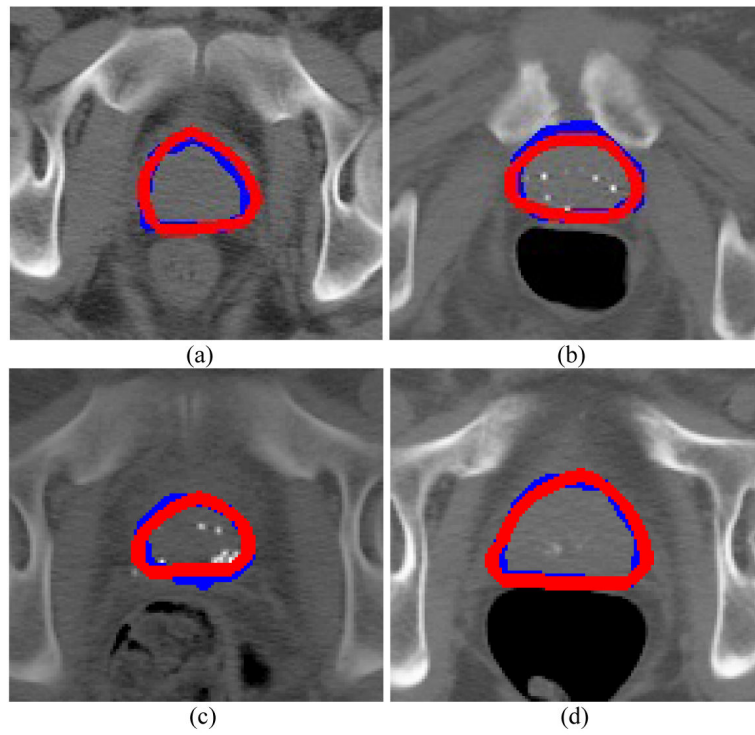


Fig. 3. The segmented prostate on the 2D slices (a)-(d). The blue and red lines mean the segmented prostates obtained by our method and manual gold standard, respectively.

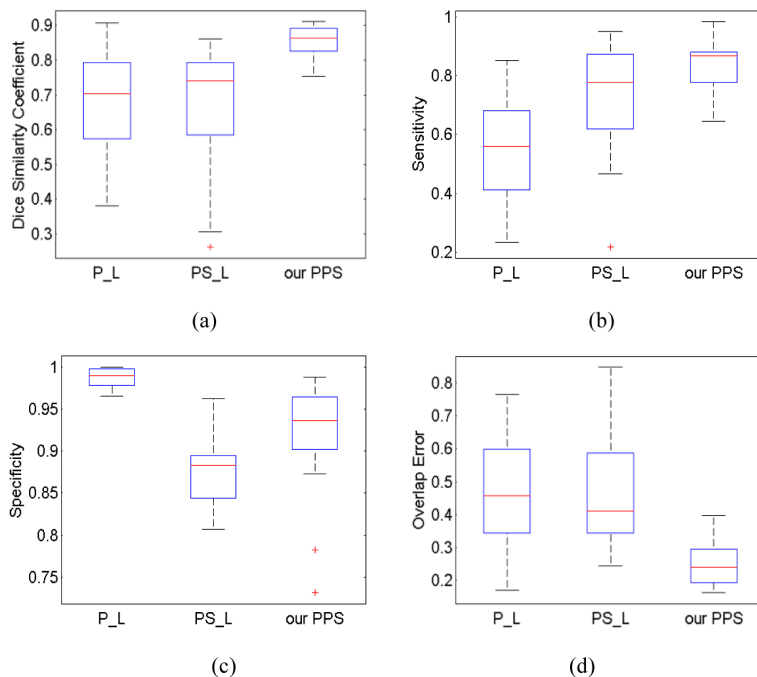


Fig. 4. The performance of the three segmentation methods: the population learning method (P_L), the patient-specific learning methods (PS_L), and our method PPS. (a) Dice similarity coefficient, (b) Sensitivity, (c) Specificity, and (d) Overlap error for the CT data of 15 patients.

The segmentation performance for the CT data of 15 patients.

Table 1

| | P1 | P2 | P3 | P4 | P5 | P6 | P7 | P8 | P9 | P10 | P11 | P12 | P13 | P14 | P15 |
|---------|------|------|------|------|------|------|------|------|------|------|------|------|------|------|------|
| DSC (%) | 87.7 | 89.2 | 82.5 | 91.1 | 87.7 | 75.3 | 89.4 | 85.6 | 85.4 | 78.8 | 89.3 | 86.4 | 75.7 | 83.4 | 89.7 |
| SE (%) | 87.0 | 87.5 | 97.0 | 86.8 | 97.1 | 64.5 | 88.2 | 78.2 | 79.9 | 81.4 | 87.5 | 77.7 | 65.8 | 72.5 | 98.3 |
| SP (%) | 90.1 | 92.5 | 87.3 | 96.4 | 78.2 | 96.5 | 90.8 | 96.8 | 93.7 | 90.9 | 94.0 | 98.3 | 94.5 | 98.9 | 73.2 |
| OVE (%) | 21.9 | 19.5 | 29.8 | 16.3 | 21.8 | 39.6 | 19.2 | 25.2 | 25.4 | 35.2 | 19.3 | 23.9 | 39.1 | 28.5 | 18.7 |